View metadata, citation and similar papers at core.ac.uk

brought to you by CORE

provided by Loughborough University Institutional Repository

This item was submitted to Loughborough's Institutional Repository (https://dspace.lboro.ac.uk/) by the author and is made available under the following Creative Commons Licence conditions.

creative commons

COMMONS DEED

Attribution-NonCommercial-NoDerivs 2.5

You are free:

- to copy, distribute, display, and perform the work

Under the following conditions:

Attribution. You must attribute the work in the manner specified by the author or licensor.

Noncommercial. You may not use this work for commercial purposes.

No Derivative Works. You may not alter, transform, or build upon this work.

- For any reuse or distribution, you must make clear to others the license terms of this work.
- Any of these conditions can be waived if you get permission from the copyright holder.

Your fair use and other rights are in no way affected by the above.

This is a human-readable summary of the Legal Code (the full license).

Disclaimer

For the full text of this licence, please go to:
http://creativecommons.org/licenses/by-nc-nd/2.5/

Application of Computational Fluid Dynamic (CFD) Simulations to Spray-Freezing Operations

C. Anandharamakrishnan[+], J. Gimbun, A.G.F. Stapley* and C.D. Rielly

Department of Chemical Engineering, Loughborough University

Loughborough, Leicestershire, LE11 3TU, UK

Correspondence: Prof. C.D. Rielly, Department of Chemical Engineering, Loughborough University, Loughborough, Leicestershire, LE11 3TU, UK. Tel:+44 1509 222504; E. Mail: C.D.Rielly@Lboro.ac.uk

[+] Present address: Central Food Technological Research Institute, Mysore-570020, India.

Abstract

A 3-D computational fluid dynamics (CFD) simulation for spray-freezing in a cold gas has been developed and used to identify design improvements. This model includes an approximate method to model the latent heat of fusion, and is able to track particle trajectories. The simulation predictions agreed reasonably well with experimentally measured gas temperatures and droplet velocities. The results suggest that a hollow cone spray is more effective in cooling the particles uniformly. The CFD simulation suggested that build up of an icy layer on the cone walls observed experimentally was due to incomplete freezing of larger particles (> 100 μm). Collection efficiencies could be raised (from 20% to 57%) by increasing the diameter of the chamber outlet.

Keywords: recalescence, solidification, residence time, impact position.

INTRODUCTION

Freeze-drying is a popular method of producing shelf stable particulate products, and is of particular value for drying thermally sensitive materials (usually biologically based), which can be heat damaged by higher temperature methods, such as spray-drying. Porous structures are formed from the creation of ice crystals during the freezing stage, which subsequently sublime during the drying stage and this often leads to good rehydration behaviour of the product. It is possible to produce freeze dried produce in powdered form using a technique known as spray freeze drying [1,2], in which a liquid stream containing a dissolved solid is atomised in a manner similar to spray drying, then contacted with a cold fluid to freeze the droplets. These are finally freeze dried, either conventionally or in a fluidised bed [3, 4, 5].

One method of spray freezing is by contacting with a cold gas. This is a complex process which involves a number of mechanisms: (i) the formation and the motion of individual drops with respect to each other and the gas is determined by the fluid mechanics of the spray, (ii) heat transfer between the gas and the droplets depends on the local conditions, *e.g.* gas temperature, droplet temperature and droplet-gas slip velocity and (iii) the freezing and ice crystallisation within the drops.

Al-Hakim [6] studied droplet size and axial velocity during spray-freezing using Phase Doppler Anemometry (PDA). However, the PDA measurements could only be performed at a maximum axial distance of 0.2 m below the nozzle. At greater distances difficulties were experienced due to (i) droplet freezing causing a reduction in refractive scatter, (ii) fewer numbers of

droplets entering the measurement volume due to spreading of the spray, and (iii) greater interference of droplets not in the measurement volume due to a generally greater degree of "fog" further away from the nozzle. However, the design and operation of a spray freezing process requires information on particle behaviour (temperature, velocity and residence time) throughout the chamber. In recent years, the rapid development of applications of computational fluid dynamics (CFD) to food processing operations has been witnessed [7, 8]. However, to date, no articles have been reported in the open literature on the CFD modelling of spray-freezing operations.

This paper deals with the development of CFD simulations of spray-freezing to predict gas and particle temperatures, velocities and residence times. The simulations can be used as a tool to improve the spray-freezing operation by determining particle velocities, temperatures and impact positions on the wall during the spray freezing process for different equipment configurations and operating conditions. Three simulation case studies for spray freezing were examined as follows:

Case A: Solid cone spray in the existing experimental geometry

Case B: Hollow cone spray in the existing experimental geometry

Case C: Solid cone spray in a modified spray-freezing chamber design

EXPERIMENTAL PROCEDURE

The experimental verification study was performed using a co-current configuration with a solid cone spray and comparison was made with Al-

Hakim's [9] data. The geometry used in this simulation is shown in Fig. 1, with a solid cone spray pressure nozzle atomiser located near the top of the chamber; the freezing gas (liquid nitrogen) enters via an annulus.

Spray freezing was carried out in the same chamber used by Al Hakim [9] (height 1.5 m and diameter 0.8 m), which included plane windows to permit PDA measurements to be made. The windows were removable to allow easy cleaning and drying of the chamber between experiments. The sprayed liquid was distilled water which was atomised using a hydraulic nozzle (WL 053), which is a solid (full) cone spray nozzle. The nozzle housings required exterior air heating to prevent blockage caused by freezing of the feed stream within the nozzle. The pressure of the liquid feed for the hydraulic nozzle was 6 bar with a corresponding liquid flow rate of 0.0125 kg/s.

The liquid feed was supplied from a pressurized feed tank to maintain constancy of flow. All feed pressures were controlled by regulator valves, which were pre-set during trial experiments to give the desired line pressures at the nozzle, and were measured using piezo transducers. The sprays were actuated on each occasion by the use of solenoid valves in the feed lines. Before spraying took place the chamber was first purged with dry nitrogen gas to remove humidity from the chamber and then cooled using a liquid nitrogen supply. During spray-freezing experiments, a chamber temperature of – 42°C was maintained by controlling the flows of liquid nitrogen. The temperature in the chamber was measured by a thermocouple and was kept within ±2°C of the desired set point. The cooling gas exit velocity was measured by a rotary vane velocimeter to be 1.5 m/s and the corresponding inlet velocity was calculated to be 0.99 m/s.

Gas Temperature Measurements during Freezing

Gas temperature measurements were performed to validate the CFD simulation predictions. Measurements of the cold gas temperature are complicated by the deposition of frozen particles on the thermocouples. Preventative steps can be taken to avoid excessive error in measurements, as described by *e.g*. Kieviet [10]. The method used here followed that of Papadakis and King [11] who used plastic caps to act as a simple shield to protect the thermocouple from the direct impact of particles. Five T-type thermocouples were spaced evenly along a plastic rod covering a region from the centre-line to the wall (the thermocouples were fixed about 10 cm apart). All five thermocouples were logged via data acquisition hardware (DataScan 7321, Adept Scientific, UK). The averaged steady-state temperature values were taken for the validation of the CFD simulation results.

Droplet Velocity Measurements

The droplet velocities were measured using a Phase Doppler Anemometer (PDA) as described in Al-Hakim *et al*. [9].

CFD SIMULATION METHODOLOGY

The CFD code Fluent 6.3 was used to simulate in 3D the co-current flow spray-freezing unit fitted with a pressure nozzle with a solid cone spray for Case A and Case C and a hollow cone spray for *Case B*. The finite volume method was used to solve the partial differential equations of the model using the SIMPLE (Semi-Implicit Pressure-Linked Equations) method for pressure-velocity coupling and a second-order upwind scheme to interpolate the variables on the surface of the control volume. For all cases

the initial droplet size distribution (DSD) was provided by a fit of the Rosin-Rammler (RR) distribution to PDA measurements of the full cone spray droplet size distribution 38 mm below the nozzle (there is no DSD available at the nozzle, since in practice it is still a liquid jet at that point). The Rosin-Rammler droplet distribution was then discretised into 16 particle size classes ranging from 0.5 μm to 250 μm (the total number of particle tracks was 1600). Two-way coupling between the cooling medium and 'inert particles' using the discrete phase model (DPM) was used; the stochastic effects of the turbulence on the particle trajectories were included through an eddy-interaction model.

The heat transfer between the droplet and the cold gas was computed based on the following equation.

$$m_p c_p \frac{dT_p}{dt} = hA_p\left(T_g - T_p\right) \tag{1}$$

where, m_p is the mass of the droplet, c_p is the droplet specific heat, T_p is the droplet temperature, A_p is the surface area of the droplet. The heat transfer coefficient, h, was obtained from the Ranz equation [12].

The current Fluent 6.3 DPM model does not include phase change during freezing (solidification). Single droplet freezing studies [13,14] indicate that freezing comprises a number of stages: (i) supercooling to below the normal freezing temperature, (ii) nucleation, (iii) recalescence, whereby rapid crystal growth occurs with a sudden temperature rise, as crystal growth liberates latent heat and the droplet warms up to the normal freezing temperature, (iv) further, slower crystal growth which is limited by heat transfer from the gas, during which some freezing point depression may occur, and

(v) once freezing is complete, cooling of the frozen particle to the gas temperature. The effect of the latent heat of fusion during the recalescence and subsequent growth stages (iii-iv) was approximated in the model by assuming solidification takes place linearly over a temperature range between 0 and -10°C. Thus, the particle pseudo specific heat capacity (c_p) value was defined piecewise: for water at T > 0°C, c_p = 4185 J/kg K; for 0 °C > T > 10 °C c_p = 35 343 J/kg K to reflect the latent heat load i.e the latent heat of ice (353 430 J/kg) divided by 10 K; and for ice at T < 10 °C, c_p = 2093 J/kg K.

Simulation Conditions

The full set of CFD input and boundary conditions is given in Table 1 and reflected the experiments performed by Al-Hakim [9]. The standard k-ε turbulence model was used, with inlet k and ε values calculated according to Langrish and Zbicinski [15]. The “escape” wall boundary condition (where particles are lost from the calculation at the point of impact with the wall) was used. In the 3-D model, a hexahedral mesh was used (typical size is 0.001m) with 180 K grid cells (preliminary tests with a finer grid showed that 180k cells was sufficient to obtain grid independent solutions for the mean velocity field) . The grid geometry is shown in Fig. 1c. To maintain the accuracy of the solution near to the nozzle a fine mesh was used (shown as a dark colour in Fig. 1c). Particles history data were extracted from the simulation results using an in-house-developed post-processing computer programme. In the following results section four particle sizes (17 μm, 50 μm, 100 μm and 150 μm) were selected to illustrate the behaviour of different particle sizes.

RESULTS AND DISCUSSION

Case A: Solid Cone Spray

Comparison between Measured and Predicted Gas Temperatures

The experimental temperature profiles of the gas are plotted in Figs. 2 a-c at axial positions of z = 0.58 m, 0.8 m and 1.23 m below the nozzle. In general, the prediction results were in good agreement with the experimental results, except in the main spray region. In the CFD model the cooling gas flow appears to have difficulty penetrating the spray region, compared to the experiment. In the experiment, however, there may be droplets of liquid nitrogen entrained in the inlet gas flow which is able to penetrate into the core of the spray, and provide significant cooling, the effect of which is not included in the CFD model. Further down the chamber at z = 0.8 m and 1.23 m (where the conical section begins) the temperature profiles flatten and the core region of higher temperature broadens as the spray fans out due to (i) evaporation of liquid nitrogen and (ii) supercooling /recalescance. Moreover, the temperature of the gas outside the core is almost uniform and it appears that most of the droplets do not penetrate into this zone. This trend was also observed by Kieviet [10] and Huang *et al*.[16]

Droplet Axial Velocity

The simulated axial velocities of droplets with different sizes from a solid cone spray were compared with Al-Hakim *et al's* [9] experimental PDA results. Droplet axial velocities were measured from the spray at a chamber temperature of – 42°C (the corresponding inlet gas temperature was –70°C) and the measurement volume was located on the centre-line of the spray at

various distances vertically below the nozzle orifice: z = 0.038 m, 0.068 m and 0.108 m. PDA data were extracted for four different size droplets of 20 μm, 50 μm, 100 μm and 150 μm. Simulation results were extracted at the same locations and for similar droplet sizes, and plotted together with the experimental results (mean velocities with standard deviation) in Fig. 3.

The predicted and experimental results indicate that the larger particles travel faster than smaller particles, since the latter decelerate more rapidly towards their terminal slip velocities, which are also approximately proportional to the square of the drop diameter [11]. The simulation results are in reasonable agreement with the PDA experimental results, especially with larger diameter particles (100 and 150 μm). The smaller diameter particles (17 and 50 μm) do not show as good agreement, but their velocities are also difficult to measure accurately with PDA.

Radial Variations of Particle Axial Velocity

Simulated radial profiles of the particle axial velocity are shown in Figs. 4 a-b along with the gas velocity profile. Simulation results at z = 0.8 m and 1.23 m only are presented here, because near the nozzle the particles have not been dispersed widely enough to cover the width of the chamber (the spray half angle is 15°). Thus no particle velocity data could be collected for these cases. At these distances the particle axial velocities were similar in magnitude to the gas velocities. However, along the centre-line of the chamber, the particle velocities were slightly higher than the gas velocities, due to higher spray feed velocity compared to that of the low gas inlet velocity. The larger particles have a higher axial velocity than the smaller ones at 0.8 m and 1.23 m from the nozzle; although all particles have the same initial

velocities, the larger particles have more momentum and take longer to decelerate. Negative (upward) axial velocities are seen near the walls of the chamber at z = 1.23 m, indicating a recirculating flow.

Particle Temperature Profiles

Predicted particle and gas temperatures along the centre-line of the spray are plotted in Fig. 5. As expected the larger particles are warmer than the smaller particles, as they cool more slowly due to their larger thermal mass per surface area. The gas temperature increases up to z = 0.4 m, but is then close to the temperature of the smallest diameter particles. At z = 1.6 m the model predicts incomplete freezing of the 100 μm and 150 μm size particles (which requires cooling to 263.15 K). However, it should be borne in mind that the centre-line gas temperatures predicted by the CFD model were higher than those measured experimentally (see Fig. 2), and this would influence the predicted particle temperatures.

The simulated radial profiles of particle temperature at distances of 0.8 m and 1.23 m below the nozzle are shown in Figs. 6 a-b. Outside the core region (0.2 m < r < 0.4 m) the droplet temperatures were much lower and corresponded to complete freezing.

Particle Residence Time Distributions

The primary particle residence time distribution (RTD) was calculated by tracking a large number of particles through the flow domain and recording the time of each particle to travel from the atomiser to a wall or to a product outlet. The time a particle spends in the drying chamber is determined by its trajectory, which in turn depend on the gas flow pattern. The RTDs of the

different size particles are shown in Fig. 7. The smaller particles have a longer residence time than the larger diameter particles and the smaller size particles almost follow the gas flow. Fig. 4 also reveals that smaller size particles are able to penetrate outside the core region, where the gas velocity was low; re-circulation of gas was also shown in that region. On the other hand, larger particles shoot through the fast flowing centre core region, to impact on the conical base or to exit via the outlet. Fig. 8 shows particle trajectories and clearly reveals that some particles are re-circulated by the gas phase and have upward velocities near to the walls.

Particle Impact Positions

A knowledge of particle impact positions is important for designing and operating spray-freezing equipment. A comparison of the simulated and experimental results for particle impacts on the chamber walls are shown in Figs. 9 a-b (top views) and Fig. 9 c-d (front views). These figures indicate that a large fraction of the particles (65%) strike the conical part of the spray-freezing chamber; 11% of particles hit the cylindrical part of the wall, and only a small proportion (22%) of the particles come directly out of the chamber. Here, an interesting point is that no particles hit the ceiling, since gas re-circulation was only observed at the bottom of the chamber (see Fig. 8). These results were in reasonably good agreement with the experimental observations shown in the photographs of Figs. 9 b-d.

An important point to note is that in these experiments a significant number of particles stick to the walls. In spray drying simulations it is generally assumed that (non-sticky) particles slide down the walls towards the main product outlet. In contrast, during our spray-freezing operations, when a

frozen particle hits the wall it tended to stick and to build an icy layer as shown in Fig. 9 b. This may be because either the ice particles (being crystalline) are rougher, or that incomplete freezing has occurred (which is likely considering the results for large particles). Hence, there is a great need to pay close attention to the design of the spray-freezing chamber to maximize the freezing efficiency, the amount of product conveyed to the outlet, and also maintaining a sufficiently cold wall temperature.

Case B: Hollow Cone Spray

The *Case A* study showed that high particle temperatures and incomplete freezing of particles were obtained at the outlet. To reduce these temperatures without changing the existing chamber design, the use of a hollow cone spray was explored using CFD simulations. In all other respects, the *Case B* simulations used the same input and boundary conditions as *Case A* (including the same spray mass flow rate and initial drop size distribution).

The radial profiles of particle velocity at axial distances of 0.8 m and 1.23 m below the nozzle are shown in Figs. 10 a-b (axial profiles are not presented as relatively few droplets travel along the centreline from the hollow cone spray). The particle axial velocities are slightly greater than with the solid cone spray, resulting in slightly lower residence times (Fig. 11). In contrast to the solid cone spray results, the hollow cone spray shows all size particles, including larger sizes, penetrating outside the core region (0.1 m < r < 0.4 m). This reduces the particle velocities (due to low gas velocity) and temperatures (due to increased residence time).

The radial profiles of particle temperatures at 0.8 m and 1.23 m below the nozzle orifice are shown in Figs. 12 a-b. These show similar results to the solid cone spray, where the larger particles have higher temperatures than the smaller particles. In the core region ($0 < r < 0.2$ m) particle temperatures are almost uniform, but if particles travel outside the core ($0.2 < r < 0.4$ m) their temperatures decrease. For example, the temperatures of 50 μm particles at $z = 0.8$ m (Fig. 12 a) were around 270 K in the core region, but about 235 K outside this region. It clearly indicates that droplets sprayed outside the core region cool to a lower temperature due to the lower warming effect from other droplets.

Case C : Modified Spray-Freezing Chamber Design

Case C explores the possibilities of modifications to the existing spray-freezing chamber design to increase the outlet product collection efficiency. Here the current chamber outlet diameter was increased to 0.45 m and simulated with the same input boundary conditions as *Case A* and also using a solid cone spray (Table 1). The simulation for Case C predicts that 57% of the particles exit the chamber at the base and only 33% of particles strike the conical part of the chamber. The remaining 10% of particles impact on the cylindrical part of the chamber. There were no incomplete particles in this system (particles of longer residence time than the simulation) since the wider outlet area reduces the extent of gas re-circulation.

Comparison of the three cases

Particle Histories

Fig. 13 compares the particle impact position data for all cases and confirms that a change to the spray-freezing design produces higher outlet particle collection efficiency. Increasing the outlet diameter in C*ase C* results in almost three times more particles recovered at the outlet than in *Case A* and *Case B*.

Outlet temperature

A comparison of the average outlet particle temperatures for the three cases is shown in Fig. 14. This clearly shows that the coldest particles are produced using the hollow cone spray (*Case B*). This may be explained by the hollow cone spray providing better contact between the spray droplets and the cooling gas compared to a full cone spray where the droplets within the spray may be "shielded" from the cooling gas bulk by the rest of the spray. This study also suggests that increasing the outlet area increases the particle temperatures due to reduced re-circulation of gas in the cone region, so although more particles are caught, fewer may be completely frozen.

CONCLUSIONS

A 3-D CFD model for spray-freezing has been developed for solid and hollow cone spray operations, and to include latent heat effects. The solid cone (*Case A*) spray predictions of gas temperature and droplet velocities agreed fairly well with the experimental results, although the model temperatures along the centre-line of the spray were over-predicted. A comparative study with a hollow cone spray (*Case B*) suggested that a hollow

cone yields lower particle temperatures and a greater extent of freezing. Nevertheless larger particles emerged without fully freezing, which would explain the build up of an icy layer on the walls observed in practice. Both the solid and hollow cone spray with existing chamber design yielded very low product collection efficiencies (<20%). The proposed redesigned chamber produces higher outlet particle collections (57%) with slightly higher temperature products.

ACKNOWLEDGEMENT

CA gratefully acknowledges the Commonwealth Scholarship Commission, UK for the award of a Commonwealth Scholarship which enabled this work to be carried out. We also wish to acknowledge the EPSRC (UK) for funding the development of the experimental rig (grant number GR/N16662).

REFERENCES

1. Malecki, G.J.; Shinde, P.; Morgan, A.I.; Farkas, D.F. Atmospheric fluidized bed freeze drying. Food Technology **1970**, *24*, 601-603.
2. Heldman, D.R. An analysis of atmospheric freeze drying. Journal of Food Science **1974**, *39*, 147-155.
3. Anandharamakrishnan, C.; Khwanpruk, K.; Rielly, C.D.; Stapley, A.G.F. Spray-Freeze-Drying at Sub-Atmospheric Pressures. Drying 2006 - *Proceedings of the 15th International Drying Symposium*, Budapest, Hungary, August 20-23, 2006; Vol. B, 636-642.

4. Leuenberger, L.; Plitzko, M.; Puchkov, M. Spray freeze drying in fluidized bed at normal and low pressure. Drying Technology **2006**, *7* ,11-719.

5. Claussen, C.; Ustad, T. S.; Strommen, I.; Walde, P. M. Atmospheric freeze drying- A review. Drying Technology **2007,** *25*, 957–967.

6. Al-Hakim, K. *An Investigation of spray-freezing and spray-freeze-drying*. PhD thesis, Loughborough University, UK, 2004.

7. Anandharamakrishnan, C. CFD applications for the food industry. Indian Food Industry 2003, *22(6)*, 62-68.

8. Norton, T; Sun, D.W. CFD - An effective and efficient design and analysis tool for the food industry: A review. Trends in Food Science and Technology **2006**, *17*, 600-620.

9. Al-Hakim, K.; Wigley, G.; Stapley, A.G.F. Phase doppler anemometry studies of spray freezing. Chemical Engineering Research and Design **2006**, *84(A12)*,1142-1151.

10. Kieviet, F.G. *Modelling quality in spray drying.* Ph.D. thesis, Endinhoven University of Technology, Netherlands, 1997.

11. Papadakis, S.E.; King, C.J. Air temperature and humidity profiles in spray drying. 1. Features predicted by the particle source in cell model. Industrial Engineering and Chemistry Research **1988**, *27*, 2111-2116.

12. Fluent Manual, 2005.

13. Hindmarsh, J.P.; Russell, A.B.; Chen, X.D. Experimental and numerical analysis of the temperature transition of a suspended

freezing water droplet. International Journal of Heat and Mass Transfer **2003**, *46*, 1199-1213.

14. MacLeod, C.S.; McKittrick, J.A; Hindmarsh, J.P.; Johns, M.L.; Wilson, D.I. Fundamentals of spray freezing of instant coffee. Journal of Food Engineering **2006**, *74*, 451-461.

15. Langrish, T.A.G; Zbicinski, I. The effects of air inlet geometry and spray cone angle on the wall deposition rates in spray dryer. Transactions of the IChemE **1994,** *72*, 420-430.

16. Huang, L.X.; Kumar, K.; Mujumdar, A.S. A comparative study of a spray dryer with rotary disc atomizer and pressure nozzle using computational fluid dynamic simulations. Chemical Engineering and Processing **2006**, *45*, 461-470.

LIST OF FIGURES

FIG.13. Comparison of particle impact positions for all three cases.

FIG.14. Average particle temperatures at the outlet (z = 1.73 m).

TABLE 1. Conditions for the CFD simulations

Inlet Gas	
Gas inlet temperature	203 K
Gas mass flow rate	0.336 kg/s
Gas velocity magnitude	0.99 m/s
Outlet Condition	Pressure outlet
Turbulence model	
Turbulence *k*-value	3.59×10^{-3} m^2/s^2
Turbulence *ε*-value	3.21×10^{-4} m^2/s^3
Liquid spray from nozzle	
Liquid feed rate (spray rate)	0.0125 kg/s
Feed Temperature	20 °C
Spray angle (full angle)	30°
Minimum droplet diameter	0.5 μm
Maximum droplet diameter	250 μm
Average droplet diameter	141 μm
Droplet velocity at nozzle exit	28 m/s
Rosin-Rammler spread parameter	3.21
Chamber wall conditions	
Chamber wall thickness	0.001 m
Wall material	Steel
Wall-heat transfer co-efficient	0.001 W/m^2K
Interaction between wall and droplet	Escape

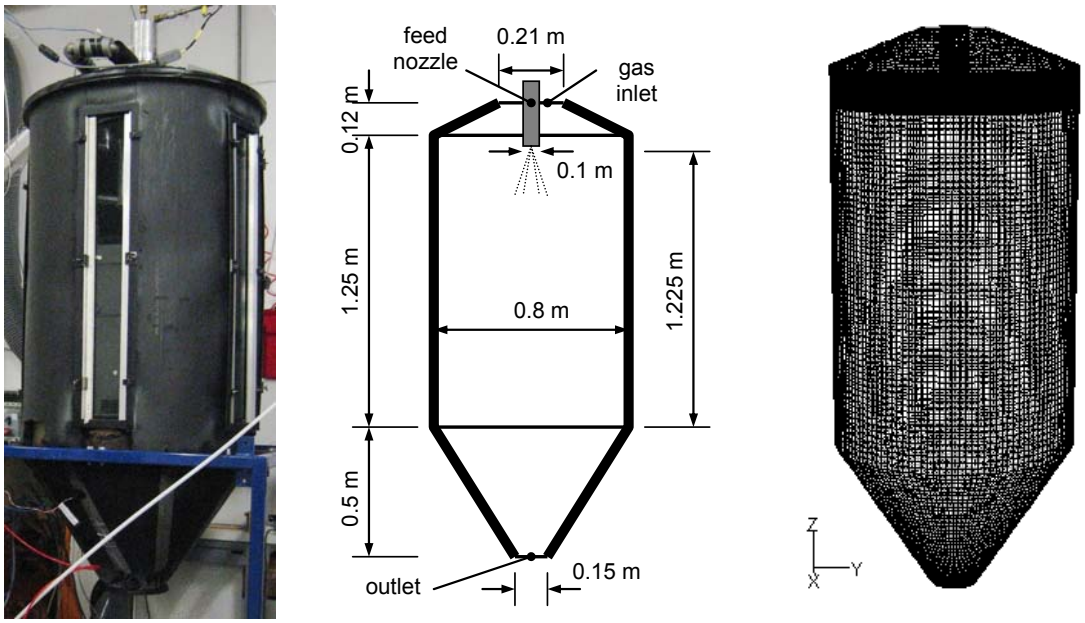

(a) (b) (c)

FIG.1. Spray-freezing chamber (a) photograph and (b) dimensions

(c) computational domain and meshing

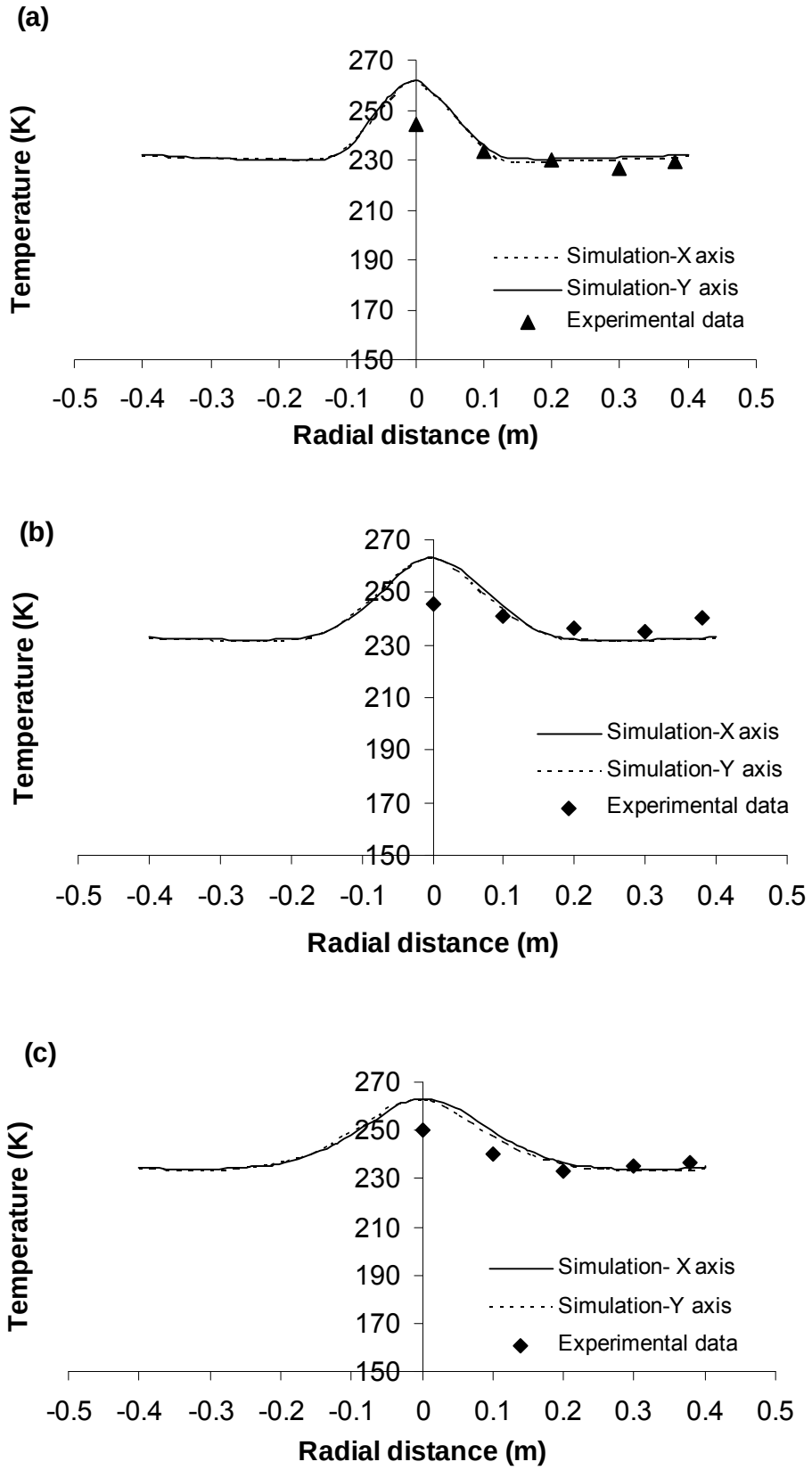

FIG.2. Comparison of gas temperature profiles between measurements and CFD predictions for Case A (solid cone spray) at (a) z = 0.58 m (b) 0.8 m and (c) 1.23 m from the nozzle spray point.

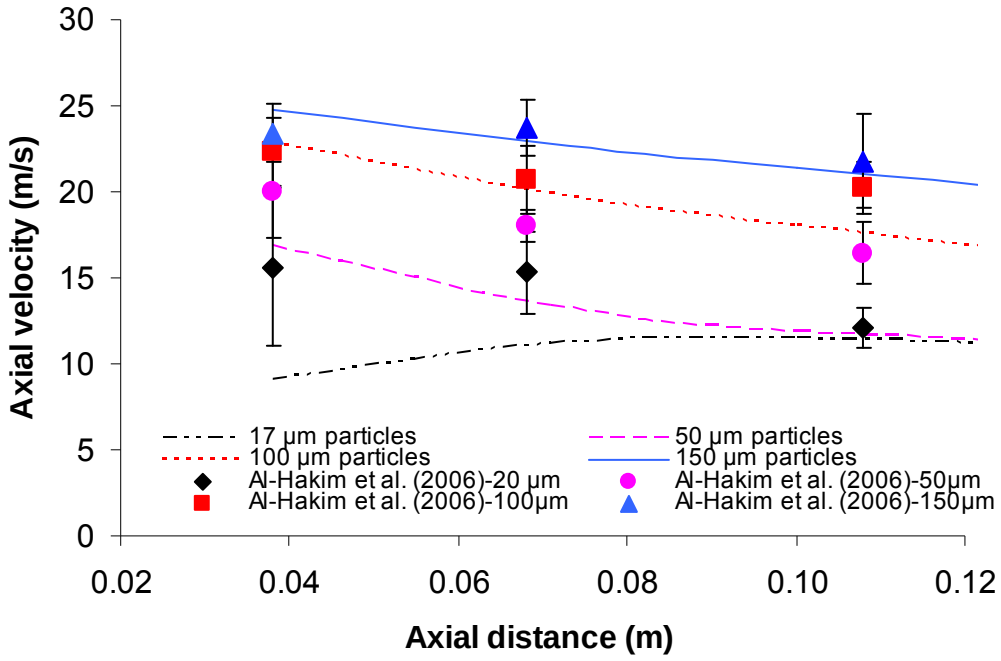

FIG.3. Comparison of axial velocity between measurements and simulation at axial distances of 0.038 m, 0.068 m and 0.108 m from the nozzle for various particle sizes (*Case A*).

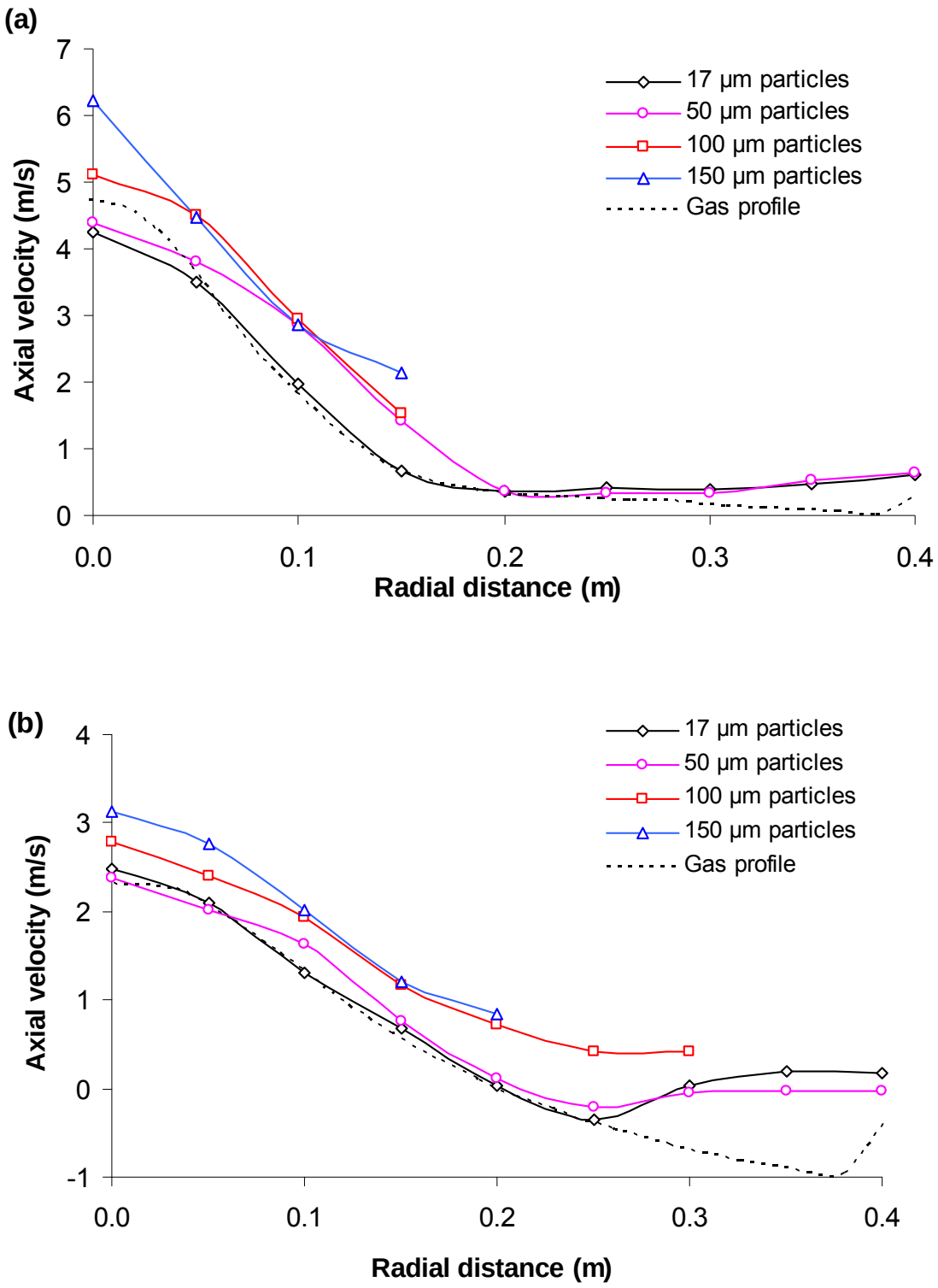

FIG.4. CFD simulated particle axial velocities at (a) 0.8 m and (b) 1.23 m below the nozzle (*Case A*).

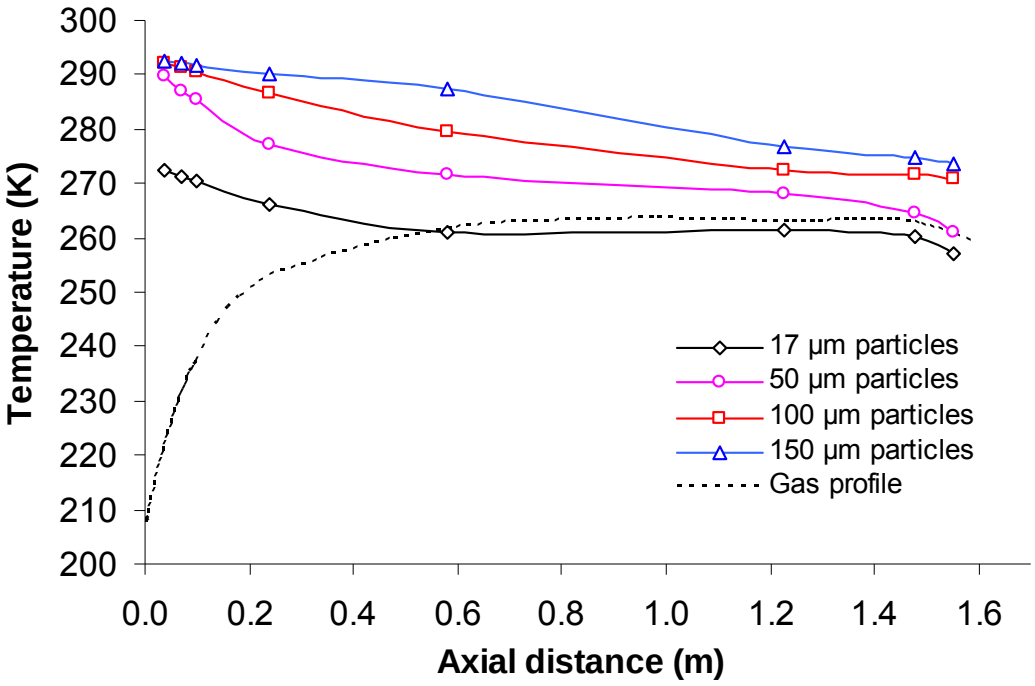

FIG.5. Variation of CFD simulated particle temperatures with axial distance below the nozzle (*Case A*).

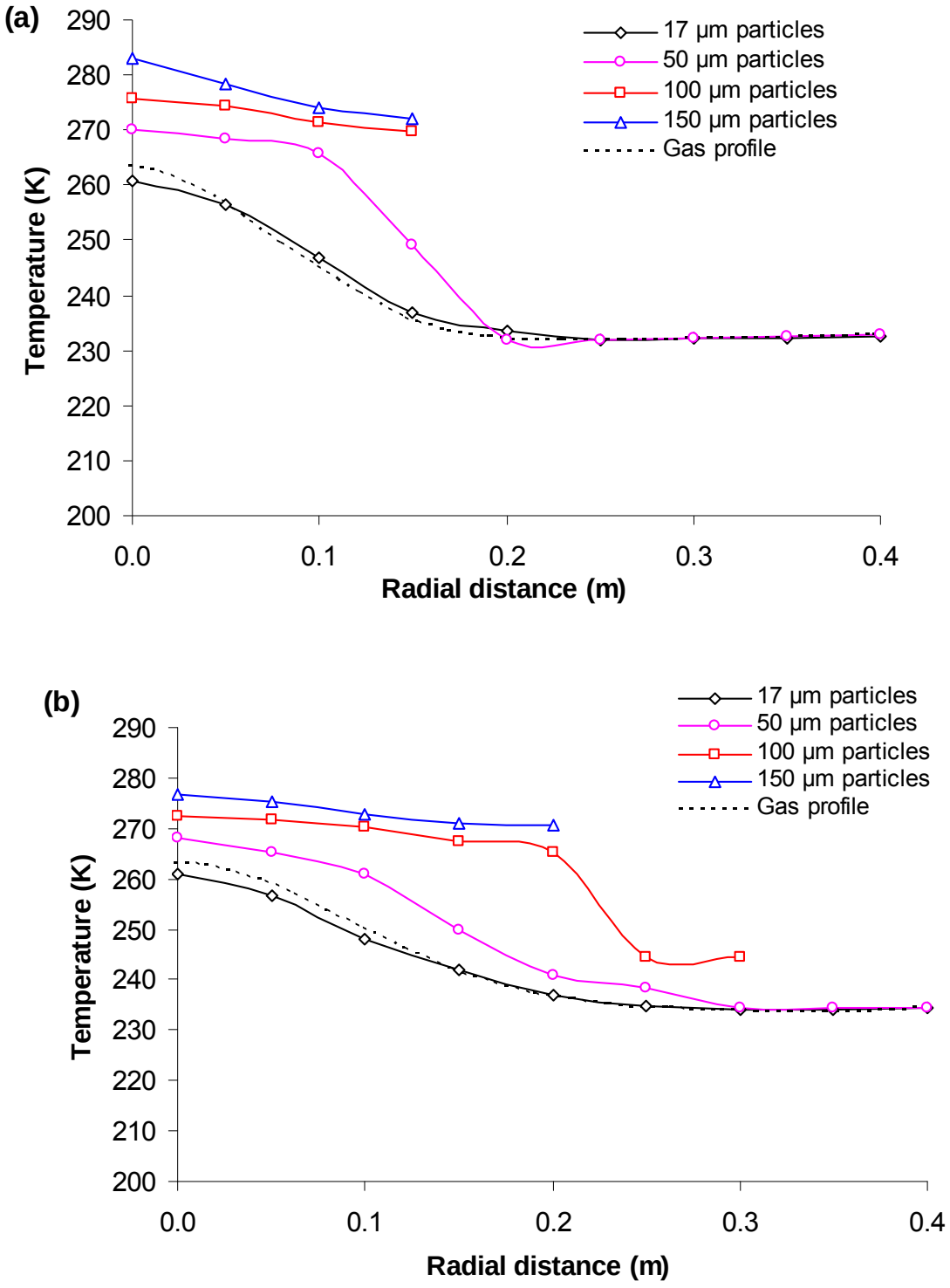

FIG.6. Variation of CFD simulated particle temperatures with radial distance at axial distances below the nozzle of (a) 0.8 m and (b) 1.23 m (*Case A*).

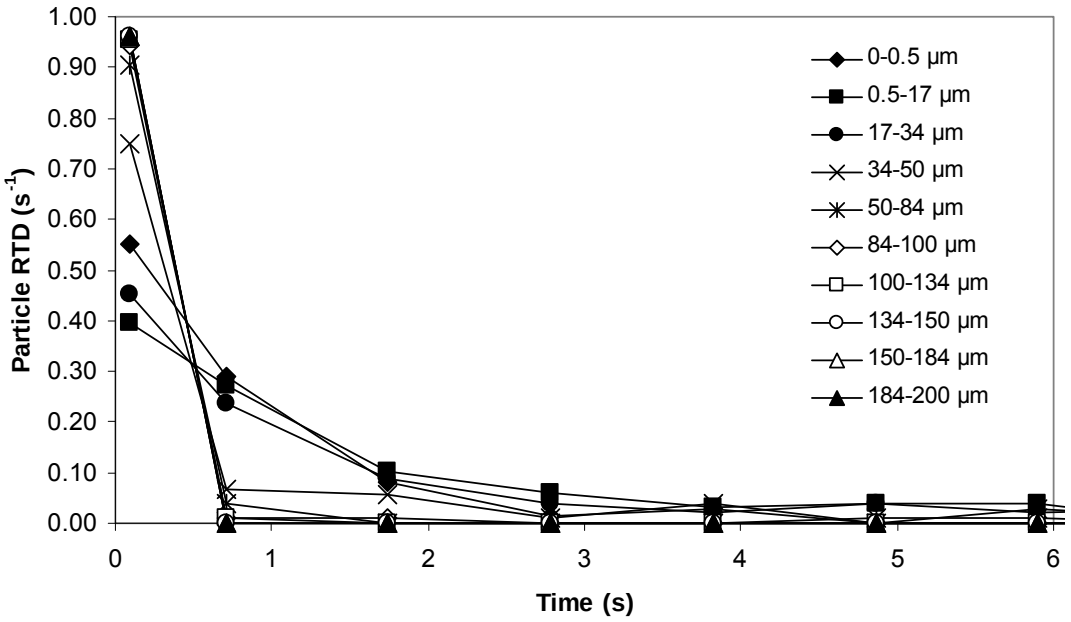

FIG.7. Predicted residence time distribution for different particle sizes (*Case A*).

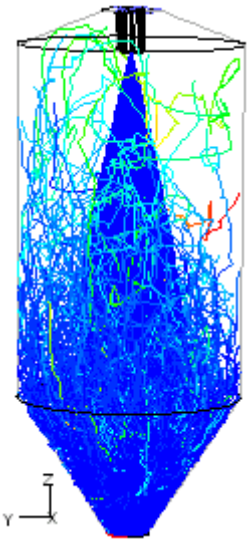

FIG.8. CFD simulated particle trajectories (*Case A*).

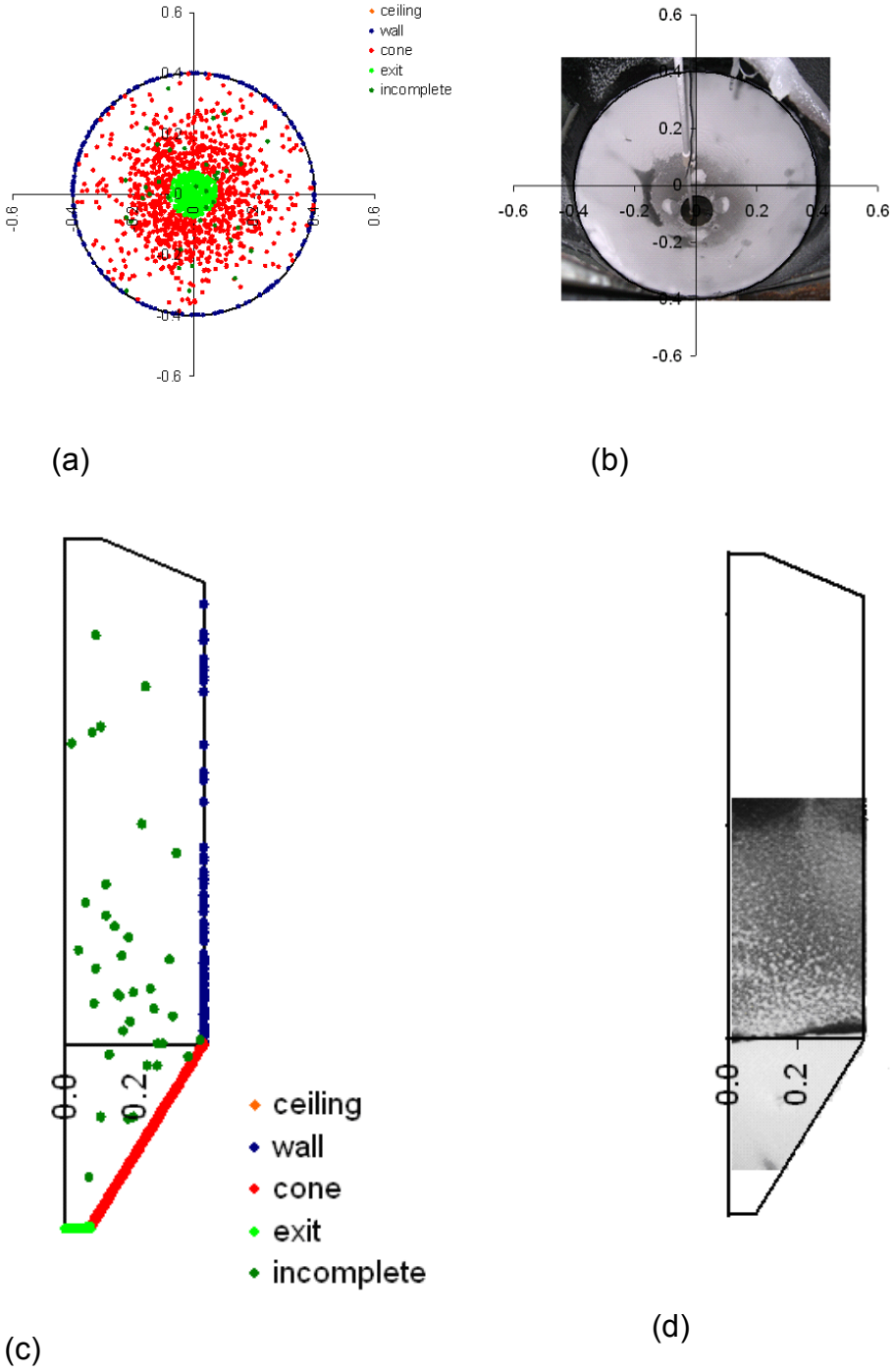

FIG.9. CFD simulated (left) and experimental observations (right) of particle impact position on the cone (a,b) and side (c,d) walls (*Case A*).

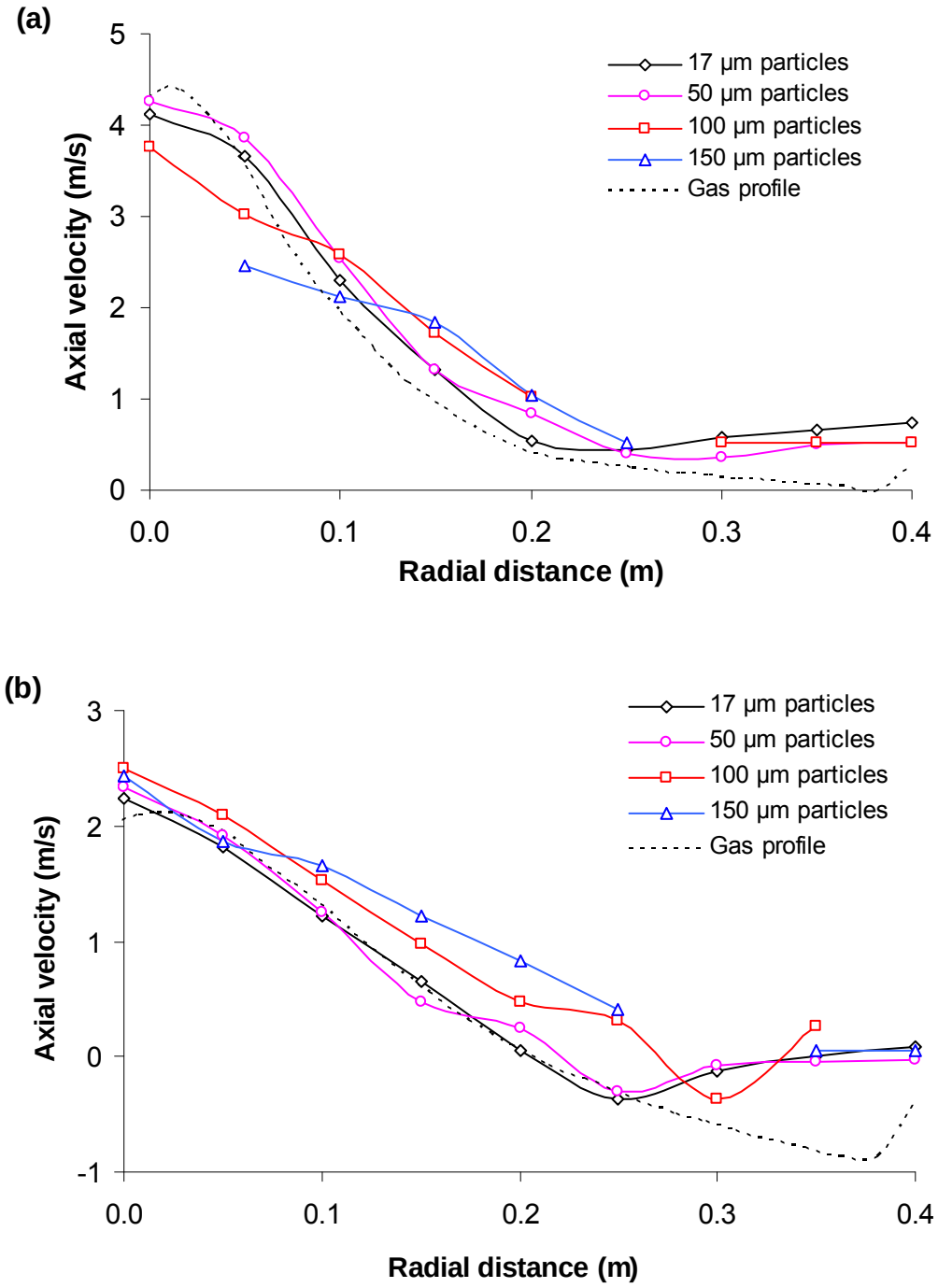

FIG.10. CFD simulated hollow cone spray particle axial velocities at axial position of (a) z = 0.8 m and (b) z = 1.23 m (*Case B*).

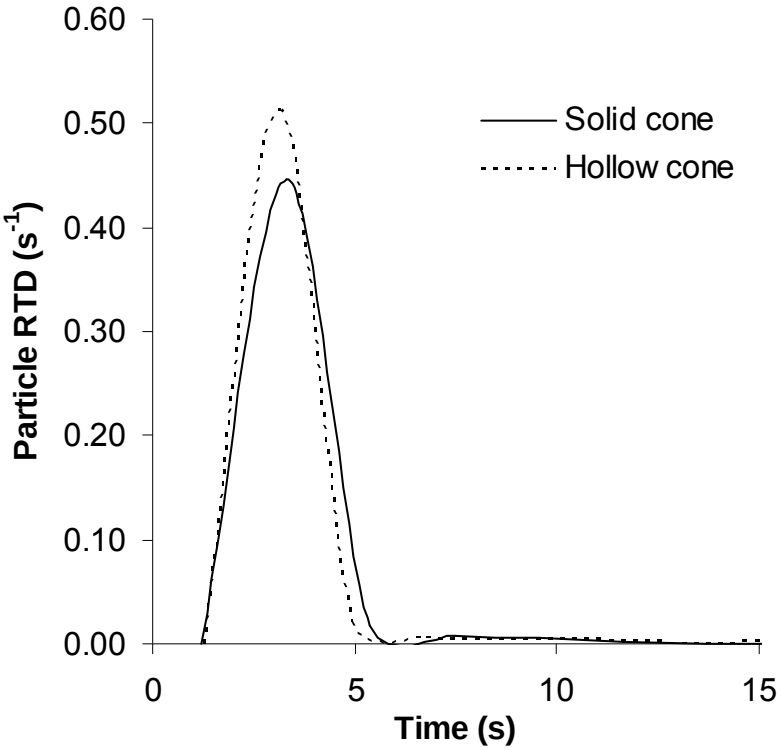

FIG.11. Comparison of solid and hollow cone spray particles overall primary RTD.

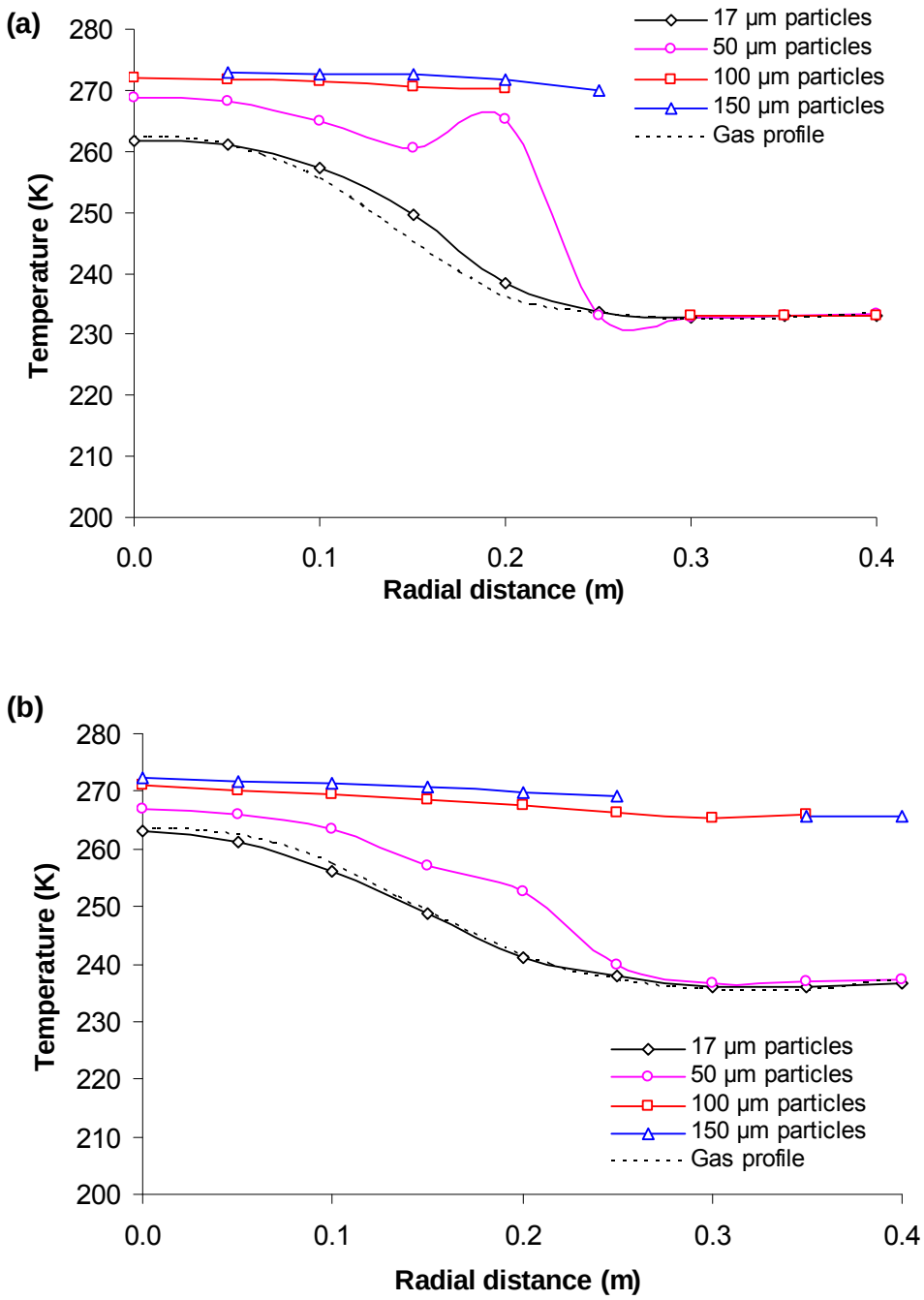

FIG.12. CFD simulated hollow cone spray particle temperatures at (a) 0.8 m and (b) 1.23 m below the nozzle (*Case B*).

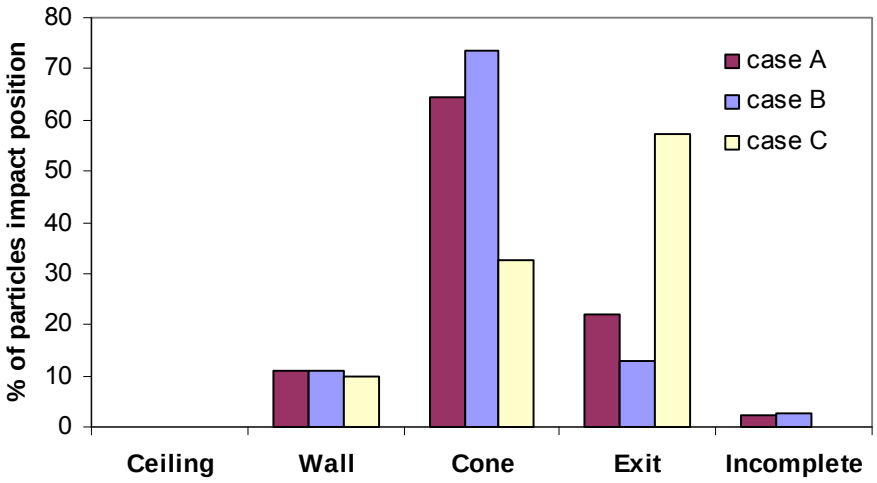

FIG.13. Comparison of particle impact positions for all three cases.

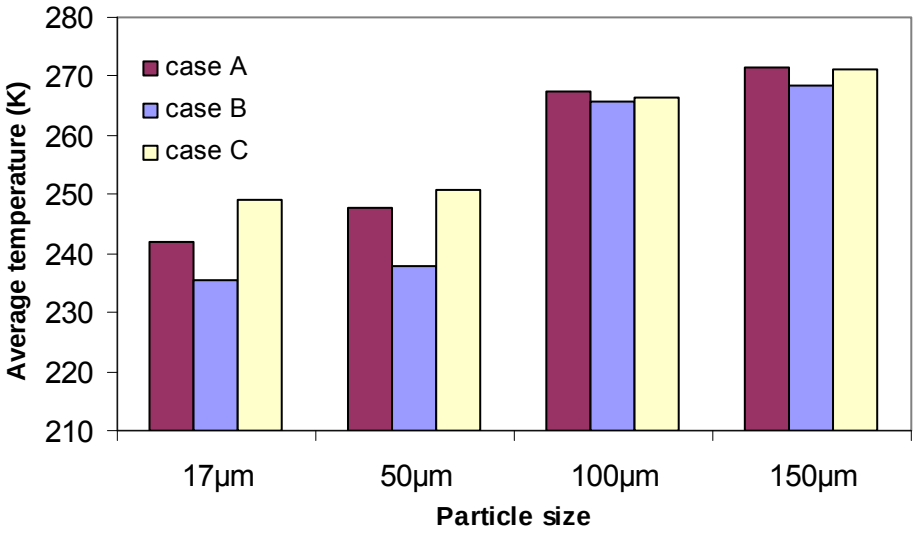

FIG.14. Average particle temperatures at the outlet (z = 1.73 m).